J. Earth Syst. Sci. (2023)132 58
https://doi.org/10.1007/s12040-023-02064-7

Characteristic differences between two contrasting tropical squalls

Chandrani Chatterjee* and Saurabh Das

Department of Astronomy, Astrophysics and Space Engineering, Indian Institute of Technology, Simrol, Indore 453 552, India.
**Corresponding author. e-mail: chandrani.chatterjee9@gmail.com*

MS received 30 January 2022; revised 14 July 2022; accepted 22 November 2022

Climatic changes and the recent surge in weather extremities are alarming concerns for society today. Tropical squall events with extremely heavy rainfall and lightning are among the very severe ones among such activities. Usually, squalls have a leading convective edge followed by a stratiform trail; however, the reverse is also observed in rare cases. This work presented a thorough study on a conventional and an unconventional squall with nearly similar severities from a tropical location, Kolkata. The study reports notably high wind gusts and lightning activities during both events, with the latter one showing higher values. The CAPE increase and OLR drops were significant in both the cases. Breakage of storm front were noticed in the first squall, which possibly resulted in higher CAPE surrounding the study location even though the localised value was slightly larger during the second event. The unconventional squall having a shorter life cycle showed weaker vertical wind shear. The cloud system during the second squall structure showed dominance of smaller cloud particles and lower cloud top pressure than the first event, whereas the cloud mask fraction and cloud water path were large in this case. The rain microphysics has been studied for the two said events and a greater number of drops has been observed in the reflectivity through region than in the stratiform phase for the squall with trailing convective line, unlike the one with conventional structure. The rain microphysical properties showed clearly distinguishable behaviour during the three phases of the squall passage for both the events. Exceptionally high a values in empirical relation between Z and R were noticed in both the cases. The study reports higher path attenuation during the first event. The study can be useful in improving the understanding of the efficiency of different atmospheric and precipitation microphysical features in the predictability of a mesoscale system.

Keywords. Tropical squall; stratiform leading edge; cloud properties; rain microphysics.

1. Introduction

The increasing number of weather extremities resulting from the recent climatic changes is emerging out to be a serious threat to human lives and resources all around the globe. The intensification of water cycle has been evidenced to correspond directly with increase in global temperature (Wang *et al.* 2017). In tropics, cumulonimbus clouds combine up to form a mesoscale system pretty often. Tropical mesoscale convective systems causing extremely heavy precipitation and thunderstorm are among the alarming severities.

Published online: 29 March 2023

India has encountered a dreadful number of severe extreme events during the last century (De *et al.* 2005). To be specific, the increase in frequency of extreme rain events with severe thunderstorms over Indian subcontinent has become a serious cause of concern in the recent past (Mishra *et al.* 2018; Carvalho and Wang 2019). It is well documented that heavy rain associated with lightning causes significant fatalities in India every year. During 2018–2019, almost 2800 people lost their lives to it (https://indianexpress.com/article/explained/explained-why-lightning-still-kills-so-many-indians-7128058/).

Convective clouds, when organised in a linear fashion, are termed as 'squall lines' (Huschke 1959). Hamilton and Arch-bold (1945) first reported rows of cumulonimbus clouds at the edge of broad downdraft region. This downdraft region in tropical squall can sometimes be as wide as 600 km (Zipser 1969). Such systems are reported to have two spells of downdraft, i.e., one narrow but intense precipitation zone and another wide but gentle rain zone (Zipser 1977). Betts (1976) derived that the mean airflow in the vicinity of the squall is a result of complex interaction between convective and mesoscale component of the squall system. Almost all squall lines usually have a prominent line of thunderstorms with moisture being supplied to them by warm air ahead of them. However, sometimes drier air intrudes due to the splitting of front and causes large thermodynamic instability, with a convective available potential energy (CAPE) > 2000 J kg^{-1} along with high wind shear (Rotunno *et al.* 1988). Therefore, the destructive properties of such a system are enormously high. Major severities due to squall events have been reported by several researchers from different parts of the globe (Moussa *et al.* 2019; Özdemir *et al.* 2019). Global Atmospheric Research Program's Atlantic Tropical Experiment (GATE) in 1974 revealed that squall events account for 50% of tropical rain, which makes it crucial even in the general circulation over tropics. This is even more severe in the recent climate change scenario as the rainfall in squall line events has been reported to be extremely sensitive to the atmospheric temperature rise (Singleton and Toumi 2013).

Understanding the microphysical structure of such a convective system is crucial in modelling and predicting the same. The cloud microphysical properties serve as excellent indicators of convection in squall mesoscale system (Makela 2004; Molinie and Jacobson 2004). Cloud top temperature seemed to affect the degree of convection negatively, whereas the columnar ice in cloud has been found to correspond positively with the lightning strike rate (Solomon *et al.* 2003). The distribution of ice particles also showed a significant impact on the number of lightning strikes (Buiat *et al.* 2017). However, the inter-relationships between convection and the cloud microphysical properties are complex and case-dependent (Betz *et al.* 2013). On the other hand, convection and microphysical parameters of rain are also reported to be strongly correlated. Raindrop size distribution (DSD) characteristics and number of lightning flashes in an event showed to correspond directly (Saylor *et al.* 2005). Therefore, a proper understanding of the microphysics, both in terms of cloud and ground rain, is crucial in the severity estimation of any squall event.

The conventional organisational mode of a squall consists of a leading convective edge followed by a wide stratiform area. However, a very rare percentage of squalls with leading or parallel stratiform edges have also been witnessed over the United States (Parker and Johnson 2000). The three classes of squalls were reported to have notably different associated environments. However, squalls with unconventional organisations are extremely rare and not well understood yet. Studies on squalls of unconventional organisational mode are very few in number, especially over the tropics.

The current work has presented a detailed synoptic and microphysical analysis of two contrasting squall line events during the year 2018. One of the squall line events was a conventional squall having a trailing stratiform edge, whereas the other one had a leading stratiform phase. A proper understanding of the associated weather variables has been attempted as well. In this paper, squall line microphysics has been reported from an ITCZ (Inter Tropical Convergence Zone) region, Kolkata (22.57°N, 88.36°E), India. Kolkata receives a large number of thunderstorms during the pre-monsoon period (Midyas *et al.* 2021; Nayak and Mandal 2014) and the city has been identified as a very highly cyclone hazard-prone area in recent reports by IMD (India Meteorological Department; https://mausam.imd.gov.in/imd_latest/contents/pdf/cyclone_sop.pdf). The rain has been measured using an optical disdrometer. The lightning measurements were retrieved by ground lightning network WWLLN. The close-range precipitation

structure has been observed with the Doppler radar images obtained from IMD. The atmospheric parameters like CAPE and measurements on the wind were obtained from ECMWF (European Centre for Medium-Range Weather forecast).

2. Data and methodology

2.1 *Event description*

Two contrasting squall line events on April 1, 2018 and April 7, 2018 have been studied in this work. One of the two squalls had a conventional organisational mode with a leading convective line followed by a stratiform tail, whereas the other showed a leading stratiform phase and a convective line following it.

2.2 *Data and instruments*

The rainfall measurement and detailed DSD (drop size distribution) observations have been made by an optical disdrometer (OTT Parsivel2) installed at Indian Statistical Institute, Kolkata. The city is situated on the bank of Hoogly River, specifically in the lower Ganges delta of eastern India (figure 1). This tropical location is located almost on the top of ITCZ line passing through the middle part of India. Kolkata has a tropical wet and dry climate, and its average annual temperature is around 24.8°C.

The mean annual rainfall is about 1600 mm here (www.imdkolkata.gov.in). Even though the city rains the most during the month of June–September due to southwest monsoon circulation but the pre-monsoon months, i.e., April–May witness several heavy rain events with thunderstorm due to the anti-cyclonic movements in the Bay of Bengal.

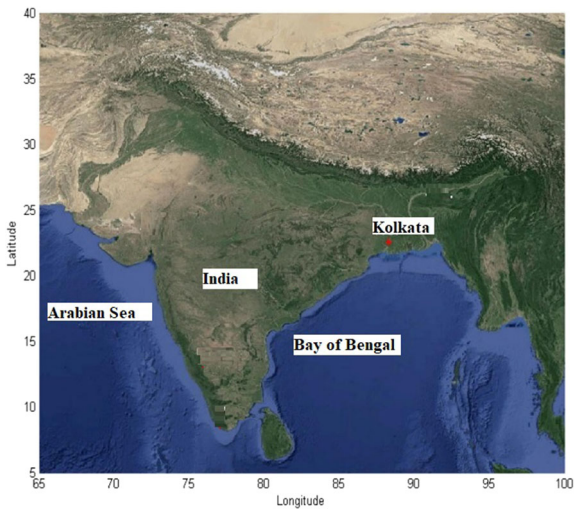

Figure 1. Location of the study area (https://www.google.com/maps).

The optical disdrometer used in this study is capable of measuring raindrop size and velocity within a diameter range of 0.062–24.5 mm and a velocity range of 0.05–20.8 m/s. The number concentration of drops is measured in 32 × 32 diameter and velocity bins. This PARSIVEL (particle size and velocity) disdrometer transmits a laser beam from the transmitter end to the receiver, and raindrops reduce its voltage by obstructing the laser beam. The reduction of voltage at the receiver end is used to determine the raindrop size, whereas the delay in receiving the signal gives an idea of the particle speed. The sampling time of the measurements has been prearranged to be 60s to get rid of any possible statistical uncertainty.

The lightning data has been obtained from the ground network WWLLN. It is operated by the University of Washington with around 70 stations spread all over the world. It uses VLF frequency band to detect the lightning location and energy in every strike (Lay *et al.* 2004). The sferic in the VLF band from three or more stations is measured during lightning strikes to compute the energy.

Wind speed and temperature data have been obtained from the automatic weather station situated at Netaji Subhas Chandra Bose International Airport, Kolkata. The airport is within an aerial distance of 6 km from the study location. Water vapour channel data were used from INSAT-3D for a large-scale view of the convective system. This recently launched meteorological satellite by ISRO can perform weather imaging in six different frequency bands. However, the close-range observation of the cloud system has been done by the Doppler radar imagery obtained at IMD, Kolkata office. IMD Kolkata comes within an areal distance of ∼20 km from the study location at the Indian Statistical Institute, Kolkata. The Doppler radar operated by IMD uses S-band frequency with a maximum scanning speed of 6 rpm and a spatial resolution of 0.25°. This radar is capable of scanning in all three scanning modes, i.e., azimuthal, elevational and volume scanning mode, but the current work has used reflectivity product MAX Z and close range reflectivity product PPI images in volume scanning mode. It provides the maximum reflectivity in north–south and east–west direction and vertical directions.

The 2.5° × 2.5° outgoing long-wave radiation (OLR) data has been procured from NOAA (Liebmann and Smith 1996), whereas real-time OLR imageries were obtained from INSAT-3DR product. The CAPE (convective available potential energy), vertical wind shear and wind gust data were obtained from ERA 5 daily dataset by ECMWF with a resolution of 0.25° × 0.25°.

The cloud microphysical properties are studied with MODIS level 3 daily gridded 1° × 1° data (Platnick *et al.* 2015).

2.3 *Methodology of analysis*

The Doppler radar imagery indicated the organisation of the squalls studied (figure 2a–b). A comparative study based on the synoptic and microphysical analysis has been carried out for the two said events.

The variation in associated weather conditions during the two events is studied first. The lightning activities, wind speed and atmospheric temperature throughout the day have been studied to figure out the change during the events, along with the wind gust during the squall passage. The degree of atmospheric instability during the event has been investigated with the help of CAPE, vertical wind shear and OLR surrounding the location of study.

The cloud microphysical properties, i.e., cloud mask fraction, optical thickness, ice particle size, cloud top temperature and ice water path, have been studied for the two said events to analyse the structural features of the precipitation systems.

Further, a comparative detailed microphysical analysis has been carried out for the ground rain as well. Lognormal model has been used here to model the DSD (Das *et al.* 2010; Vidyarthi *et al.* 2011) and given by Timothy *et al.* (2002)

$$N(D) = \left(\frac{N_T}{\sigma D\sqrt{2\pi}}\right)\exp\left[-\frac{0.5(\ln D-\mu)^2}{2\sigma^2}\right], \quad (1)$$

where $N(D)$ is the number density of raindrops (in m^{-3} mm^{-1}), N_T is the total number of raindrops, D is the raindrop diameter (in mm), μ and σ are the mean and standard deviation of $\ln(D)$. Here, the lognormal model is preferred over gamma model, because DSD parameters used in this model have very clear physical meaning. Method of moments technique is used here for computing the three basic parameters of lognormal model N_T, μ and σ because of its linear relation with the moments of DSD and the 3rd, 4th and 6th moments are considered for estimating the DSD parameters as follows (Kozu and Nakamura 1991):

$$N_T = \left[\frac{1}{3}(24L_3 - 27L_4 + 6L_6)\right], \quad (2)$$

$$\mu = \frac{1}{3}(-10L_3 + 13.5L_4 - 3.5L_6), \quad (3)$$

$$\sigma^2 = \frac{1}{3}(2L_3 - 3L_4 + L_6). \quad (4)$$

The mean volume diameter is calculated as:

$$D_m = L_4/L_3, \quad (5)$$

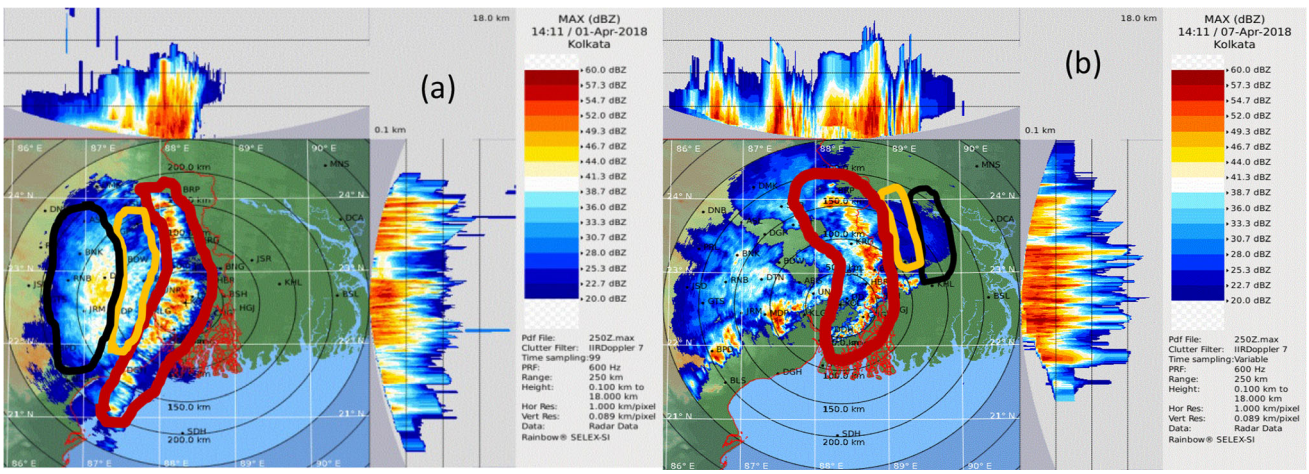

Figure 2. Doppler radar image of the precipitation system developed during the squall line events on (**a**) April 1, 2018 and (**b**) April 7, 2018 (red-convective line; yellow-reflectivity trough; black-stratiform edge).

where L_3, L_4 and L_6 are the natural logarithms of 3rd, 4th and 6th moments, respectively. The rain integral parameter Z is obtained from the DSD (Ippolito 1986).

The behaviour of all the microphysical parameters has been studied for all the phases of the event. The convective–stratiform separation has been done based on Tokay and Short (1996). Rain attenuation is estimated using Mie scattering theory, assuming spherical shape and 303 K medium temperatures.

3. Results and discussion

3.1 *Synoptic description of the events*

3.1.1 *Squall with leading convective edge*

The first squall event studied here, took place on April 1, 2018. The Doppler radar imagery serves as an excellent mode of studying the evolution of a mesoscale precipitation system (Mukhopadhyay *et al.* 2009). Here, the close-range radar observations were used to investigate the genesis of the precipitation system (figure 3a–c). The Doppler radar image at 19:40 local time showed presence of a high reflectivity (52 dBz) cloud line above the study location (figure 3a). After the passage of the convective line, a low reflectivity short-lived region was visualised over the study location, which had very low reflectivity cloud cover in some portions and clear sky in the rest (figure 3b). Figure 3(c) indicated a stratiform cloud cover with moderate radar reflectivity. It is to be noted that the close-range Doppler imagery used above do not represent the entire system overview but was necessary to have a closer observation of the study location. The squall system had a higher reflectivity gradient at the front side of the convective line (figure 4) than the back side, as reported by Dalal *et al.* (2012).

The said event has shown a short leading convective phase of rainfall followed by a wider stratiform rain (figure 5). The rainfall started at local time 19:40 and the convective phase continued for 45 minutes. The maximum rain intensity during the convective edge was found to be 79.30 mm/hr. The convective spell was followed by a very short-lived reflectivity trough region. The stratiform trailing edge started at 21:00 local time and continued for a temporal span of 1 hour and 50 minutes. The total downpour was accounted to be 19.7 mm. The length scale of the system was about 400 km while it had an active life cycle of ∼3 hr.

3.1.2 *Squall with leading stratiform edge*

The second squall event was witnessed on April 7, 2018 over Kolkata was a short-lived squall with a rare organisational mode. It showed a leading stratiform phase followed by a convective line. The close-range Doppler imageries during the three different phases of the event have been depicted in figure 6(a–c). The cloud coverage over the study location at a local time 17:50 was found to have moderate reflectivity values, which seemed to correspond for the stratiform phase of the events (figure 6a). After the completion of the leading strartiform edge, a low reflectivity trough ('T') region was observed over the location of study. The

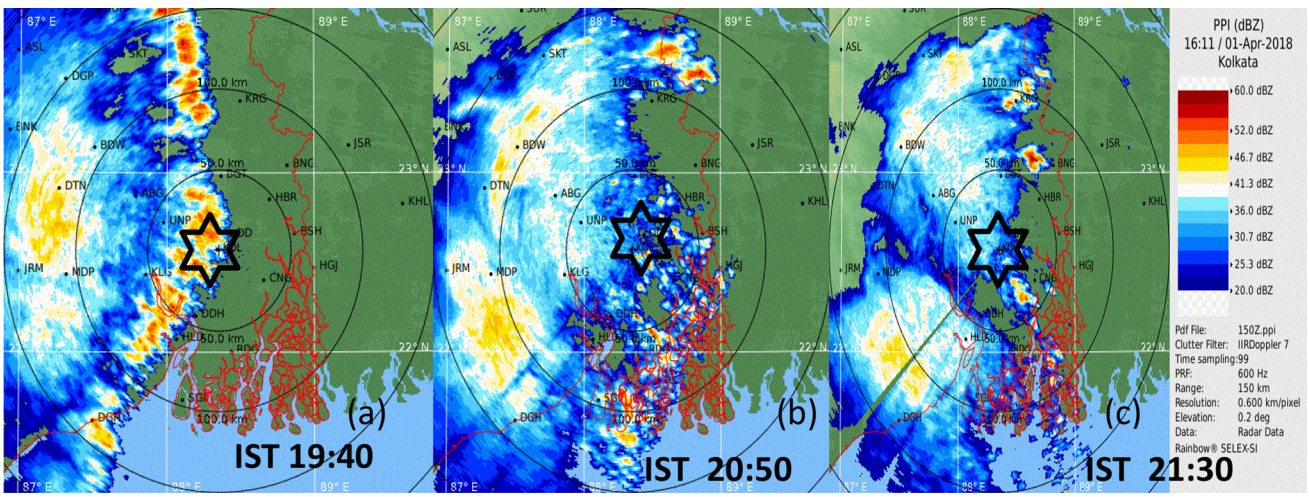

Figure 3. Close-range Doppler radar images during the three phases of the events. (**a**) Convective, (**b**) T region, and (**c**) stratiform on April 1, 2018.

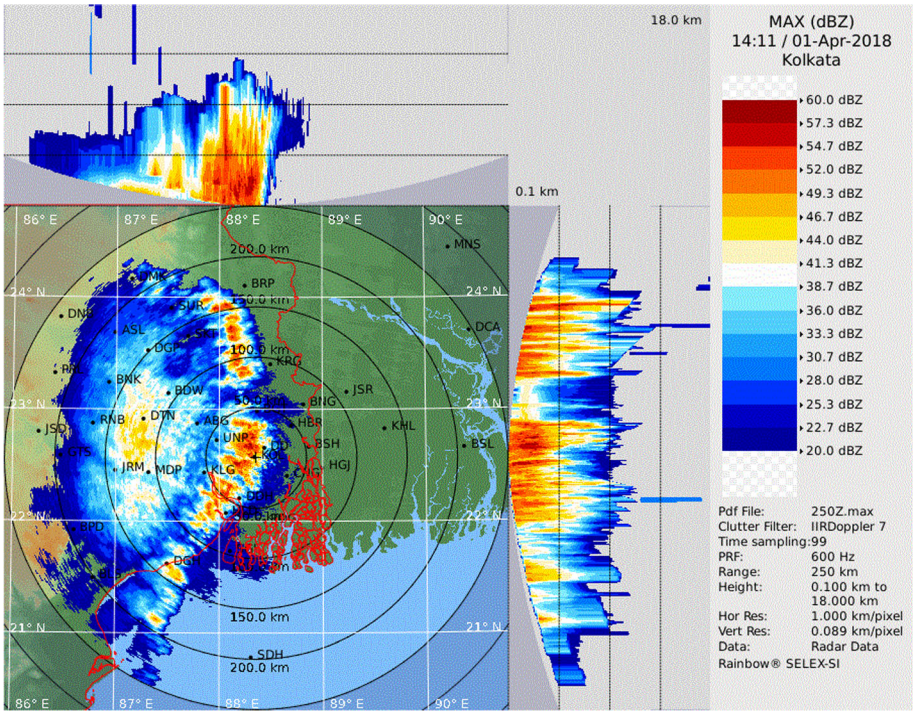

Figure 4. Doppler images showing the inter-phase reflectivity gradient on April 1, 2018.

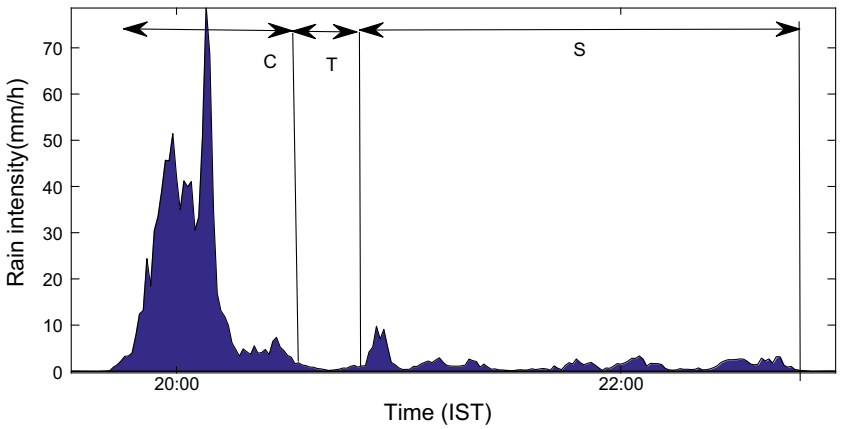

Figure 5. The variation of rain intensity during the squall event on April 1, 2018.

radar return at local time 18:20 was found to be much lower than earlier (figure 6b). The T region has been succeeded by a high reflectivity region (figure 6c). The close-range Doppler imagery at local time 19:00 indicated a convective cloud cover with high-intensity return over the study location (figure 6c). Here, the reflectivity gradient at the back side of the convective squall line was higher, i.e., between convective line and clear sky, whereas the front side of the convective line has a lower gradient of reflectivity, i.e., between a stratiform and convective cloud line (figure 7). The above organisation finds good agreement with the results reported in Dalal *et al.* (2012).

The rainfall started at 17:50 local time with a stratiform spell which continued for 25 minutes (figure 8). A reflectivity through (T) region followed this phase which lasted for 15 minutes. The most intense phase of the event started at 18:30 local time. The convective phase had a maximum rain intensity of 90.67 mm/hr and a temporal span of 23 minutes. Even though the event was very short-lived, the total rain amount was found to be 20.01 mm. The length scale of the system was

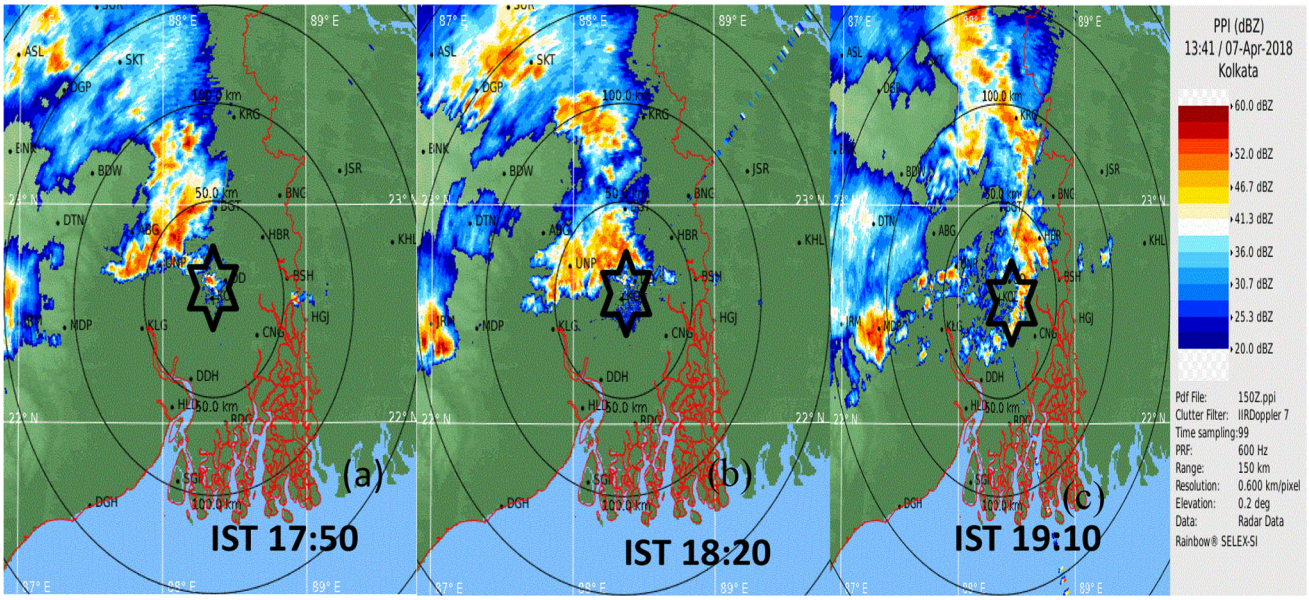

Figure 6. Close-range Doppler radar images during the three phases of the events. (**a**) Convective (**b**) T region, and (**c**) stratiform on April 7, 2018.

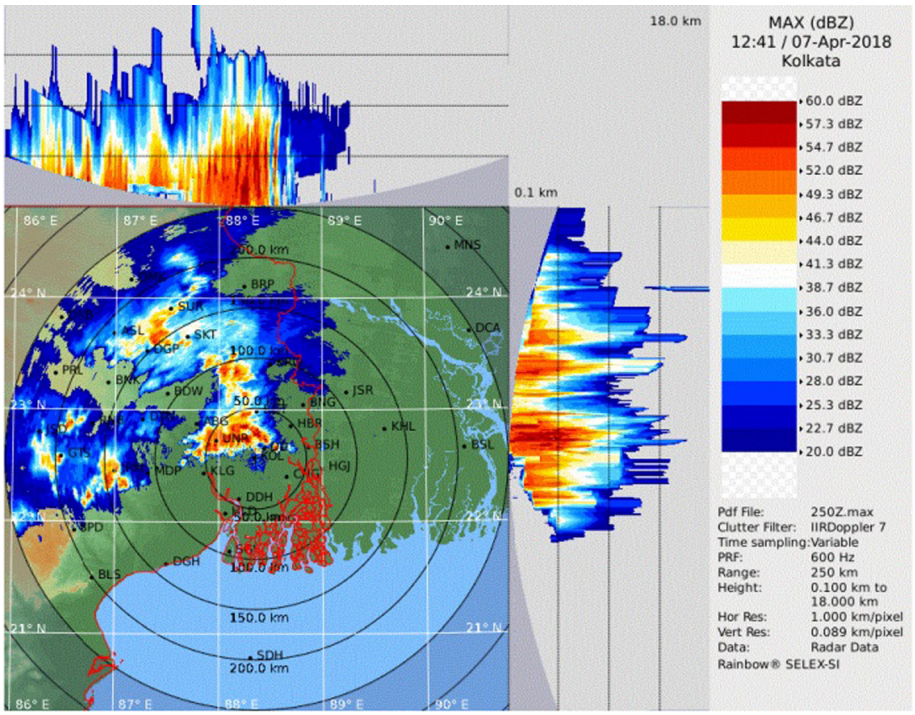

Figure 7. Doppler images showing the inter-phase reflectivity gradient on April 7, 2018.

about 250 km while it had an active life cycle of ∼2 hr.

3.2 *Comparative study*

3.2.1 *Weather conditions*

Significant lightning activities were witnessed by Kolkata and its surroundings during both the squall events. Figure 9(a–b) presented the spatial distribution of cloud-to-ground lightning strikes within 1° × 1° regions surrounding Kolkata during the two squall events. However, the lightning activity was even more denser during the second event on April 7, 2018 as noted with the temporal distribution (figure 10a–b). The lightning strike density reached a maximum value of 38 during the first event, whereas it was found to be 65 for the

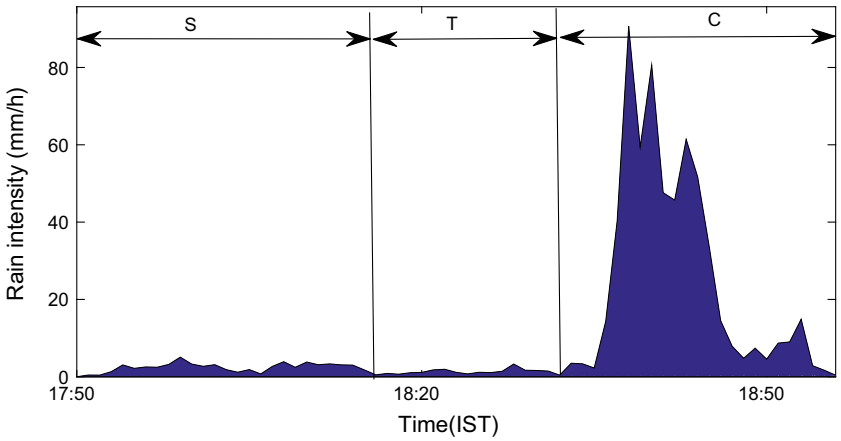

Figure 8. The variation of rain intensity during the squall event on April 7, 2018.

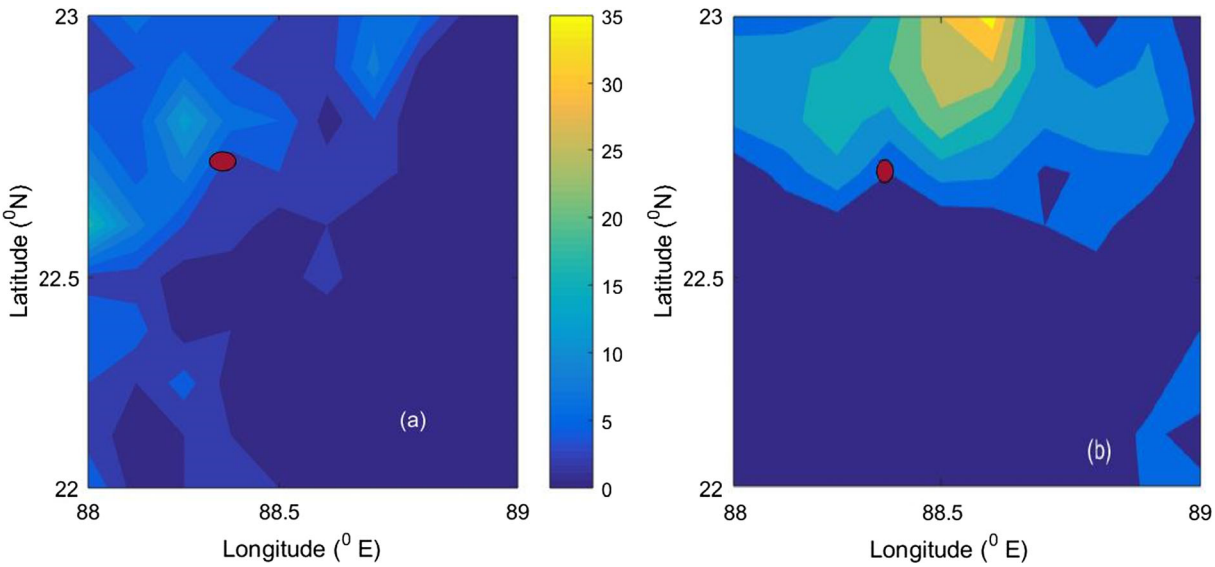

Figure 9. Spatial distribution of lightning activities during the squall events on (**a**) April 1, 2018 and (**b**) April 7, 2018.

second one. However, it is imperative to mention that the maximum density of lightning was observed at the beginning of the first event as the event started with an intense convective edge, whereas the peak lightning activities for the second event was witnessed around 18:30 local time, i.e., initiation of the convective phase.

The third element, after the lightning strikes and downpour that contributes the most to the severity of a squall, is probably the wind turbulence. The wind speed seemed to start rising with the initiation of the events and continued to be high throughout the entire span (figure 11a–b) during both the squall events.

The maximum wind speed during the two events was found to be 33.6 and 44.8 km/hr, respectively. The atmospheric turbulence at the height of 10 m above the ground was found to be high during both the events (figure 12a–b). The wide areal span of the convective system during both the squalls might have a role in high wind gust (Chaudhari *et al.* 2010). Even though the maximum wind gust experienced by the city and its surrounding was comparable during the two events (66.14 and 69.18 km/hr, respectively), the spatial distribution of wind gust showed increased turbulence over a wider areal span during the second event.

The variation in atmospheric temperature on the squall days was studied to see whether the squall had caused any temperature change in the city. Significant temperature drop has been noticed in the city after the passage of both the squalls (figure 13a–b). The first squall resulted in a

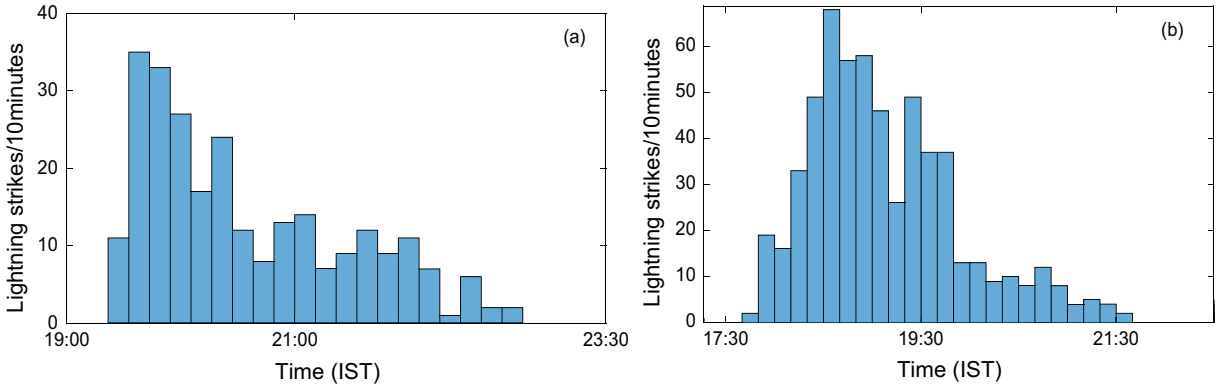

Figure 10. Temporal distribution of lightning activities during the squall events on (**a**) April 1, 2018 and (**b**) April 7, 2018.

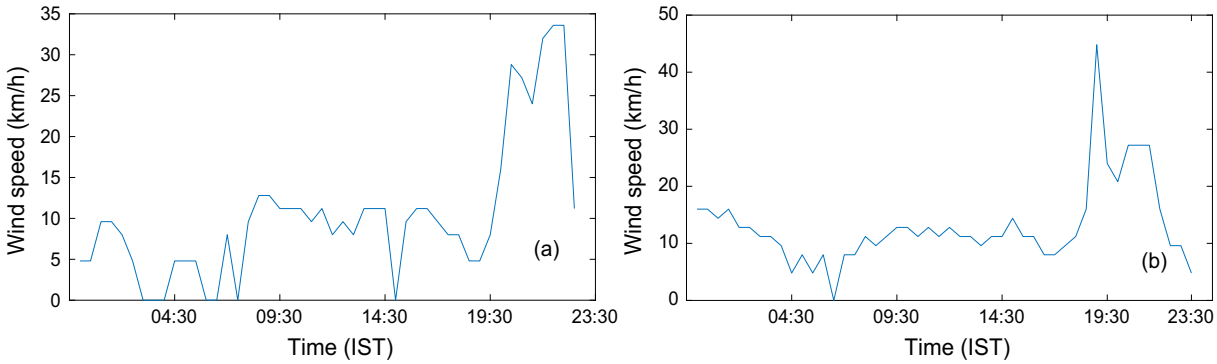

Figure 11. Rise in wind speed during the squall events on (**a**) April 1, 2018 and (**b**) April 7, 2018.

temperature drop of 7°C after the main phase of the event (figure 13a). The latter showed a sharp decrease of 10°C after the passage of the convective line (figure 13b).

3.2.2 *Analysing the status of conventional elements used in prediction of mesoscale system, during the two squall events*

Atmospheric instability and moisture are the two key ingredients in predicting the severity of deep moisture convection (Johns and Doswell 1992). However, the association is not always very straightforward (Pucik *et al.* 2021). Therefore, understanding the connection between these factors and the severity of a convective system can facilitate better prediction of the severities. A detailed analysis has been carried out here to visualise the status of the conventional factors used to study convection during the two said events. CAPE, OLR and vertical wind have been studied here for the said purpose. Figure 14(a–b) depicts the water vapour count as obtained by INSAT satellite during the events over the study location. Both the events witnessed notably bright signature in water vapour channels over the location, with higher returns during the second event (figure 14c). The results fall in line with higher downpour and lightning activities during the second event (Schiro *et al.* 2016).

Presence of a high (>2000 J kg^{-1}) CAPE value was reported to be linked with the severity of the tropical squall systems (Rotunno *et al.* 1988). Figure 15(a–b) shows the spatial distribution of convective available potential energy (CAPE) over Kolkata during the two said events. The CAPE value of the study location was found to be 3322 J kg^{-1}, whereas it was 3356 J kg^{-1} before the second event. This finds good agreement with denser lightning activities during the second event. Interestingly, a wider belt of high CAPE has been observed surrounding the study location during the first event. The CAPE distribution surrounding the study location further confirmed it (figure 15c). The breakage in the squall front during the first event has probably (figure 2a) caused more intrusion of drier air resulting in greater instability (Rotunno *et al.* 1988). On the other hand, the

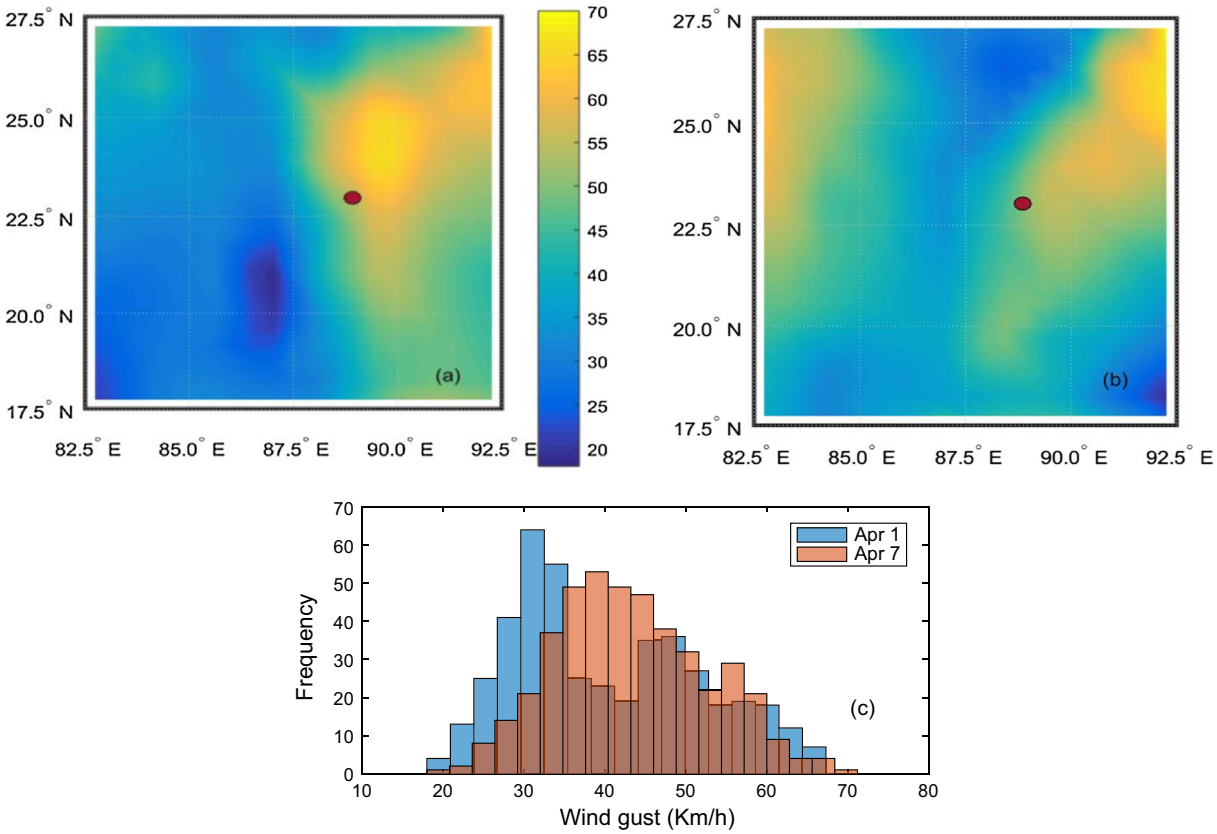

Figure 12. Spatial distribution of wind gust (km/hr) surrounding the study location during the squall events on (**a**) April 1, 2018, (**b**) April 7, 2018, and (**c**) distribution of wind gust for the two events.

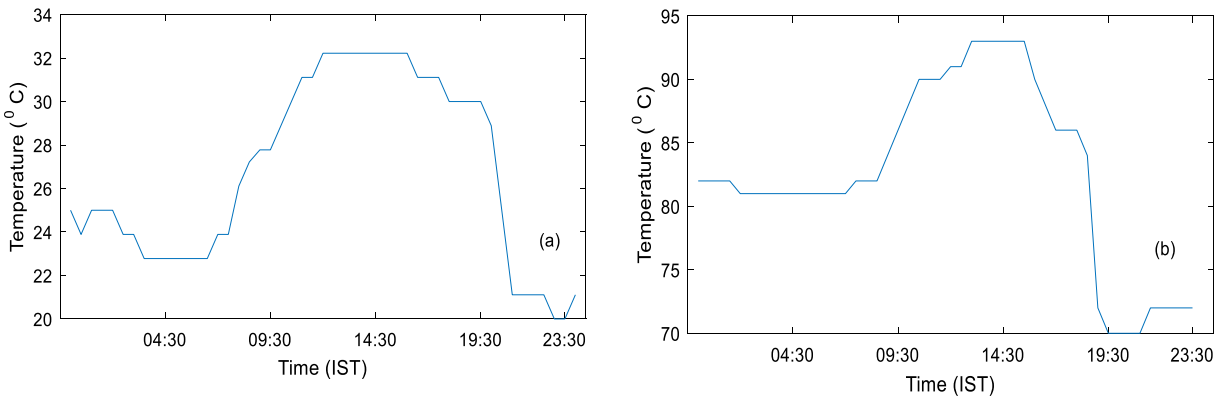

Figure 13. Atmospheric temperature during the events on (**a**) April 1, 2018 and (**b**) April 7, 2018.

squall line with the leading stratiform edge had no breakage in the convective line.

The vertical wind velocity has been studied next to understand the atmospheric instability within 400–950 hPa. Figure 16 shows the time series of vertical wind speed in different pressure levels averaged over a 3°×3° area around the study location. A maximum vertical wind velocity of 0.8 Pa/S was observed during the event on April 1, 2018 in upward direction within a pressure range of 500–400 hPa. The highest vertical wind observed during the event on April 7, 2018 is ∼0.4 Pa/S. The said occurrences of maximum speed were noted during the initial stage of the first event, whereas it was observed in the later phase of the second event. The organisation of the convective line supports the same. Interestingly, the wind speed shear (gradient) between the pressure levels looked stronger throughout the range of 400–950 hPa during the first event. Convective storms

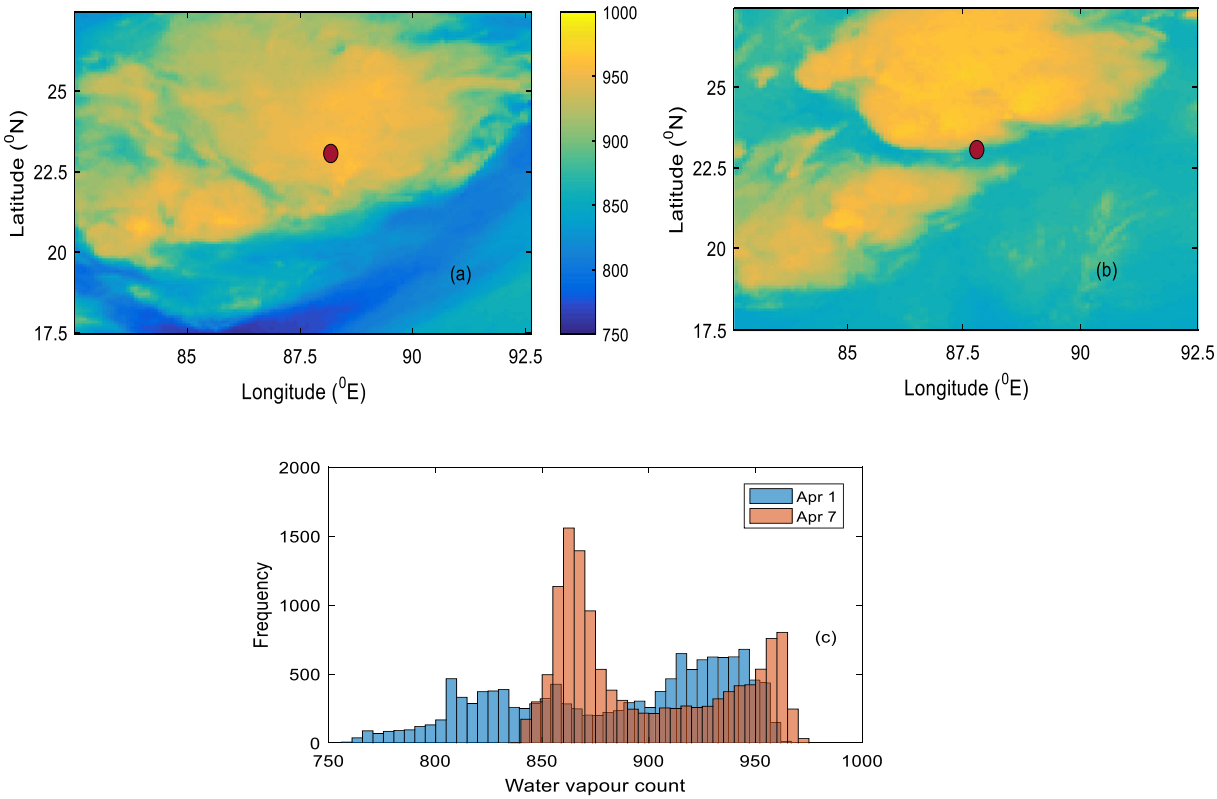

Figure 14. The convective systems developed during (**a**) April 1, 2018 and (**b**) April 7, 2018 retrieved by INSAT satellite in water vapour channel. (**c**) Distributions of the water vapour count.

develop in both strong and weak vertical wind shear, but long-lived, well-organised convection requires strong vertical wind shear (Pucik *et al.* 2021). The first squall event was a far more long-lived one having a total development and activity period of 7 hr with a 3 hr active squall which falls in line with vertical wind shear observed. Marwitz (1972) showed that rain efficiency corresponds negatively with wind shear in storms across the United States, probably due to high entrainment into the updraught and subsequent evaporation of hydrometeors. Besides, the storms often travel faster in case of environments of stronger shear, which can also be a reason behind less rain. The second squall having a greater rain amount supports the previous findings. Prediction of evolution and intensity of convective events with weak wind shear is extremely tough (Pucik *et al.* 2021). An unconventional organisational structure of the squall system probably contributes to the compromised efficiency of wind shear in predicting the severity of a system.

Outgoing long-wave radiation (OLR) is a vital component of the earth's radiation flux and can signify the overall condition of the global atmospheric system. A low OLR (i.e., 240 W m^{-2} or less) distribution indicates convective activity and plays a crucial role in identifying the location of a tropical mesoscale system (Nakazawa 2006). Figure 17(a–b) depicts the average daily OLR on the events' days. A low OLR region is evidenced over the study location on both the occasions, but the second event showed a greater drop of OLR surrounding the location of the study. The average OLR over the city fell down to 200.1 W m^{-2} in the first squall event. The OLR value was found to be as low as 172.1 W m^{-2} on the second event day. Even though the second event dropped even more OLR, both values were notably significant. The distribution of OLR confirms the same (figure 17c).

3.2.3 *Cloud microphysics*

In-depth knowledge about the microphysical structure of the convective system is extremely crucial to understand and predict weather severities. Several studies have reported strong correspondence between convective activities in a mesoscale system and cloud microphysical parameters (Makela 2004; Molinie and Jacobson 2004). However, the variability of such correlation seemed to be case-dependent. Environmental conditions

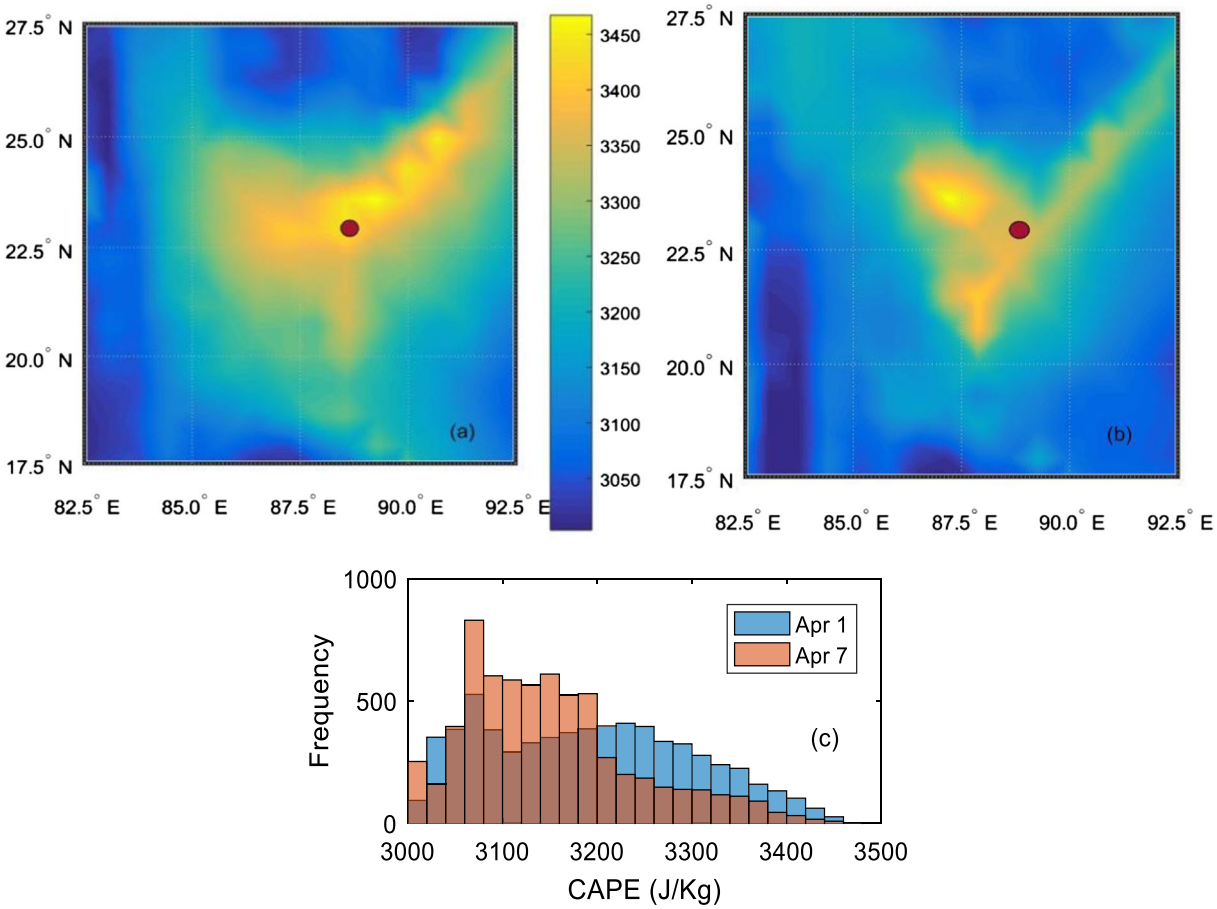

Figure 15. Spatial distribution of CAPE (J/kg) surrounding the study location before the squall events on (**a**) April 1, 2018 and (**b**) April 7, 2018. (**c**) Distribution of CAPE for the two events.

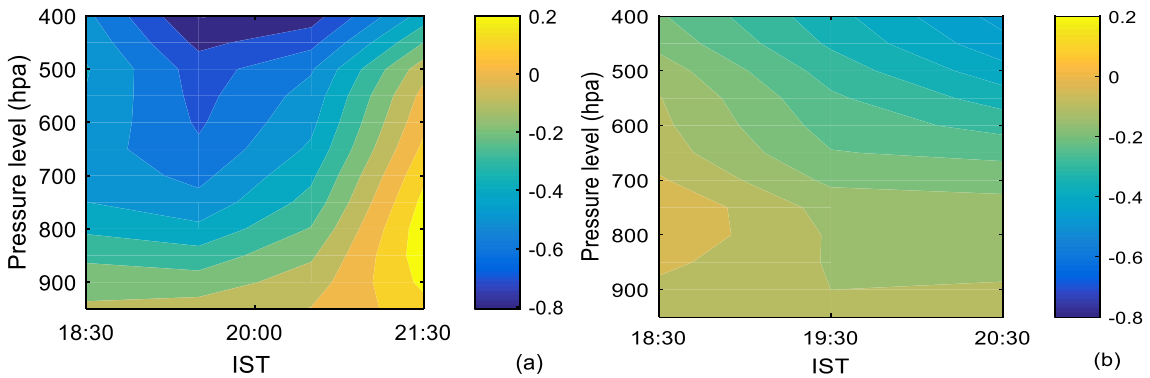

Figure 16. Wind velocity (Pa/S) in different pressure levels during the squall events on (**a**) April 1, 2018 and (**b**) April 7, 2018. The (–) sign signifies upward air motion.

and initial perturbation responsible for cloud stimulation also can modulate them significantly (Betz *et al.* 2013). The current work has studied squalls of two different organisational modes. Therefore, it was important to investigate the association between microphysical properties of the precipitation systems and the severity of the convective line.

The distribution of cloud mask fraction (figure 18a) showed dominance of denser cloud masks surrounding the location of study during both the squall with leading stratiform edge showing slightly higher values which fall in line with the more number of lightning strikes observed during the event (Zhao *et al.* 2017). The cloud optical thickness has been reported to show a linear

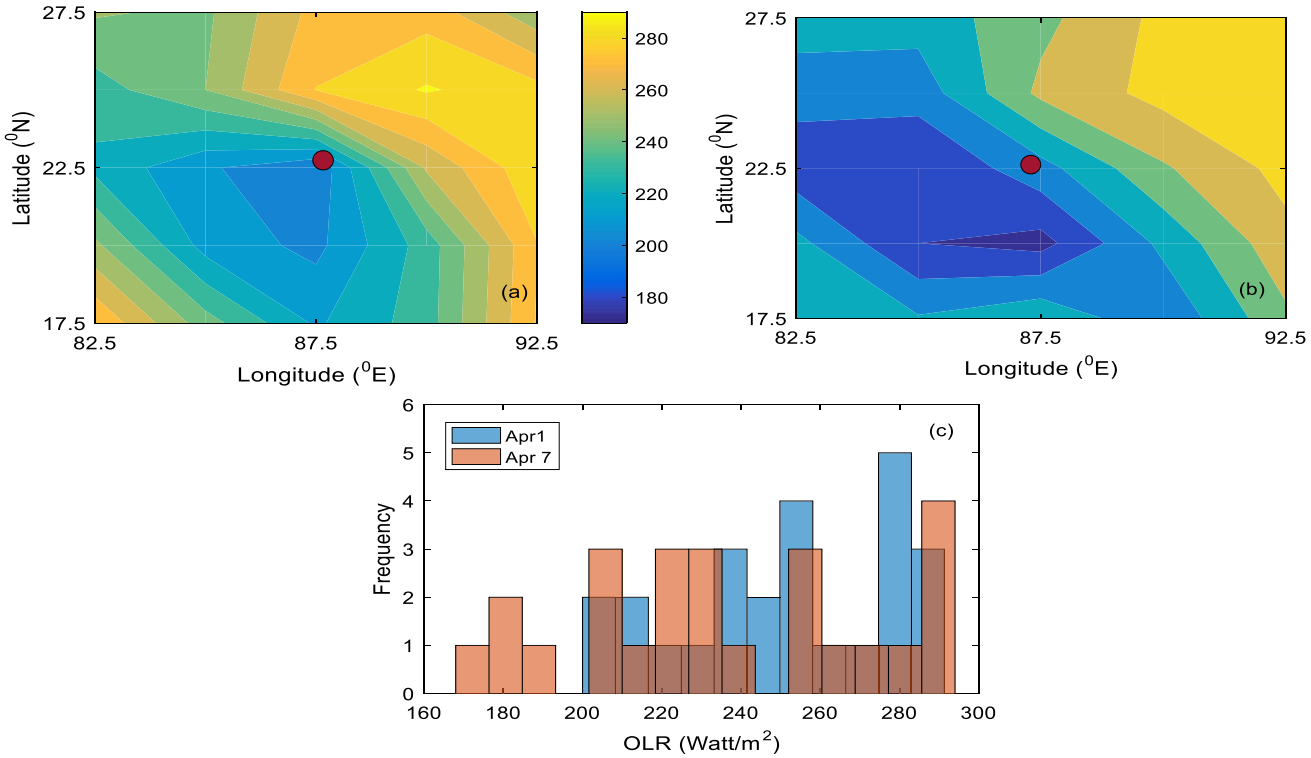

Figure 17. Spatial distribution of mean OLR (W/m^2) surrounding the study location on (**a**) April 1, 2018 and (**b**) April 7, 2018. (**c**) Distribution of OLR for the two events.

correspondence with the convection of a mesoscale system (Zhao *et al.* 2017). The highest value of cloud optical thickness during the second event surrounding the location of the study was found to be 63, whereas a maximum value of 41 was noticed in the first case (figure 18b). The breakage of ice droplets into smaller particles provides the basis of lightning due to its nature of positive charge acquisition. Therefore, smaller ice particle size in the precipitation growth phase indicates greater convection and lightning activities (Chatterjee and Das 2020). The squall event observed on April 7, 2018 showed dominance of smaller ice particles with the smallest of 10 microns ice droplets being present in the system, which finds good agreement with the heavy rainfall and thunderstorm witnessed in the event (figure 18c). Drop in cloud top pressure has been found to correspond linearly with severity of lightning activities (Altaratz *et al.* 2010). Figure 18(d) indicates the distribution of cloud top pressure over Kolkata and its surroundings during the two said events. The second squall system seemed to have a lower cloud top pressure over the location, reaching 200 mb. The cloud ice path showed notably high values during both the squalls, while the one with leading stratiform edge showed slightly larger values (figure 18e).

However, it is important to mention that the different cloud microphysical parameters used in predicting the severity of a convective system studied here, have shown good correspondence with the system severity in both the cases. Even though the comparative study has presented stronger indication of convective activity during the second activity, that should not outshine the goal of looking at the efficiency of different cloud features in the prediction of mesoscale severity during both the events reported.

3.2.4 *Rain microphysical properties*

The above analysis has pointed towards the severity of the mesoscale systems formed and the associated synoptic weather conditions during the evolution of the processes. The rain microphysical properties have been studied next to have a deeper insight into the precipitation process. The log-normal parameters N_T, μ, σ and mean rain volume diameter (D_m) have been modelled for the two events. Figure 19(a–b) shows the variation of the microphysical properties in the three phases of the events. In each case, the reflectivity pattern and rain rate criteria (Convective: $Z > 38$ dBz and $R > 10$ mm/hr) have been obeyed for the rain type

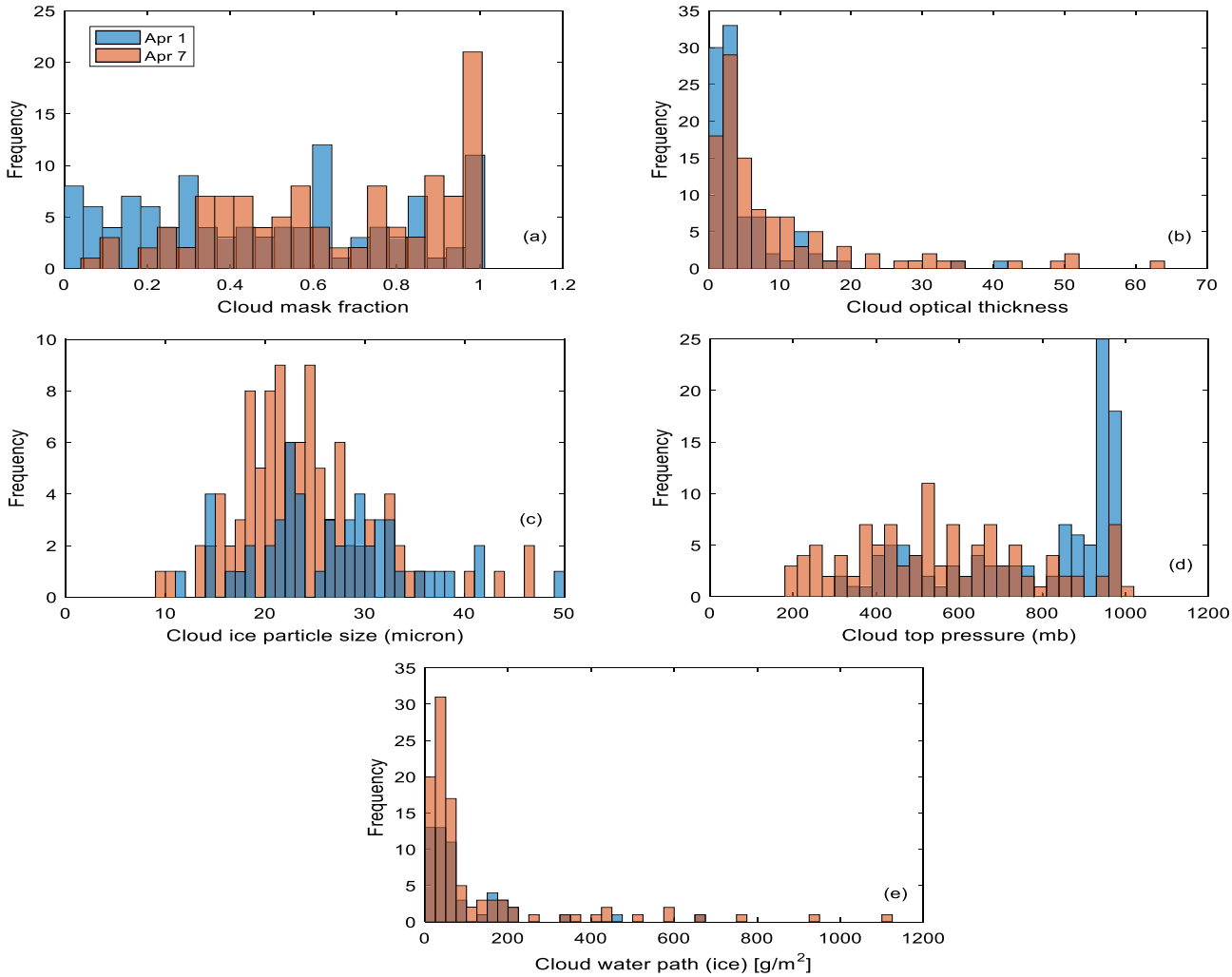

Figure 18. Distribution of cloud properties during the two events (**a**) cloud mask fraction, (**b**) cloud optical thickness, (**c**) cloud ice particle size, (**d**) cloud top pressure, and (**e**) cloud water path.

classification. The radar reflectivity during the convective phase of the first squall event was found to be high, with a maximum value reaching 58.1 dBz. The value of Z was higher in the stratiform phase than in the T region.

The leading convective edge has resulted in larger mean volume diameters in the initial stage of the first squall, which dropped significantly in the reflectivity trough (T) region (figure 19a). The stratiform tail caused the diameter to increase thereafter. However, the difference in mean volume diameter in convective and stratiform phases of the event was notable. The total number of drops was highest in the convective phase and had the lowest value during the T region. A similar signature was noted in σ. The values of μ were largest during the convective phase which was followed by the stratiform edge.

The behaviour of Z and D_{m} in different phases of the unconventional squall was pretty much in line with that of the first squall (figure 19b). However, the total number drops were highest in this event's convective phase, followed by the T region. μ was comparable in the convective and stratiform rain phases with a much lower figure in T region. The σ, however, increased significantly during the trailing convective phase and was found to be the lowest in the T region.

The implications on total number of drops are further supported by the number concentration of the two events studied separately for each of the three phases (figure 20a–b). It is evident that the convective phase consisted of large drops ranging up to 5.5 mm, whereas stratiform spell had drops within around 3 mm of diameter for both the events. The overall number concentration of the convective phase was significantly higher than the two other spells for the events. However, the reflectivity trough had the lowest number concentration in the conventional squall studied, but it

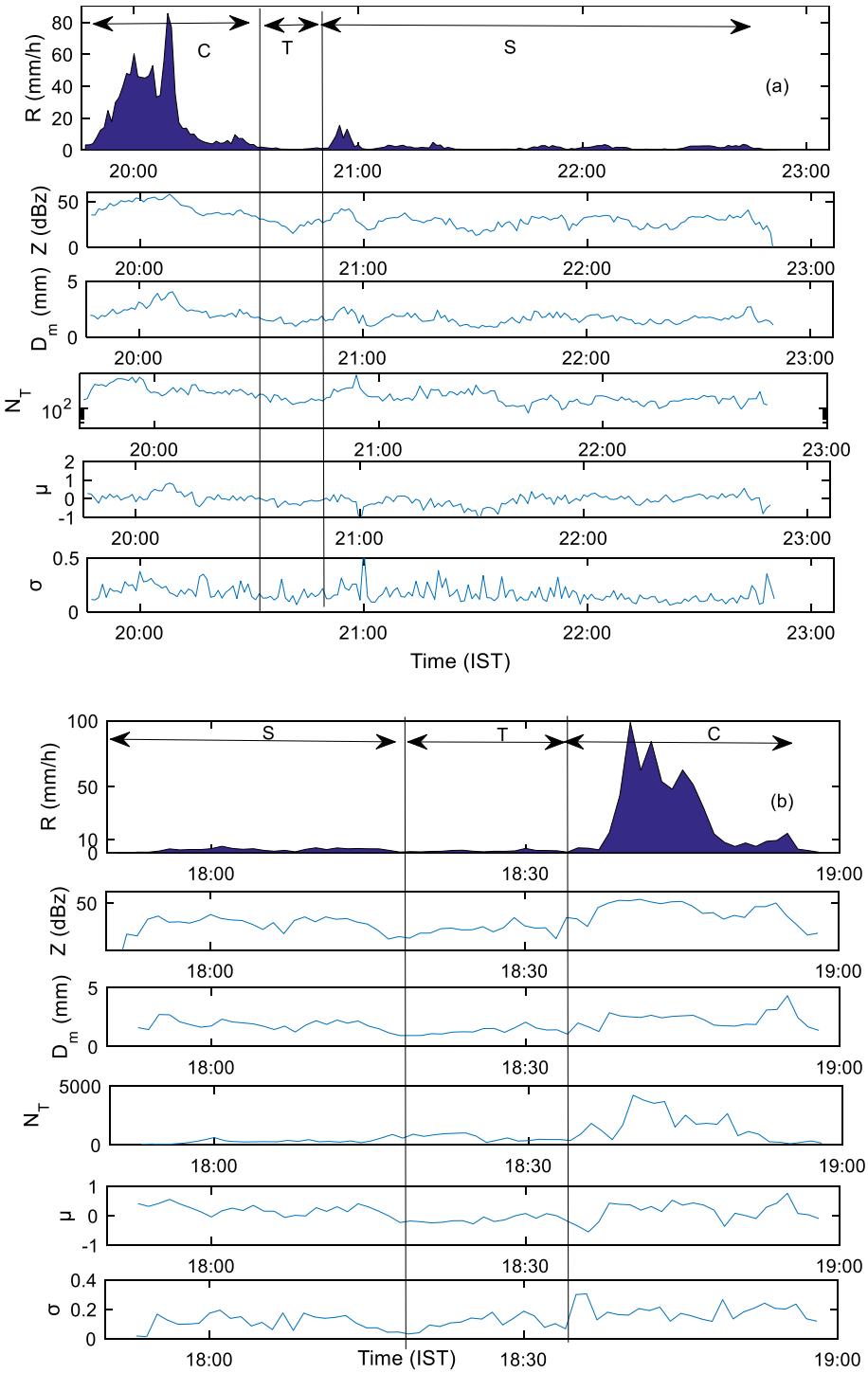

Figure 19. Rain microphysical properties of the squall events on (**a**) April 1, 2018 and (**b**) April 7, 2018.

showed more number of drops than the strartiform phase in the squall with leading stratiform edge. Larger drops were seen in the T region of the first event in comparison with the second one.

The overall event-wise variation of the log-normal parameters between the two events are shown in figure 21(a–d). The distributions looked significantly separable for the three microphysical parameters N_T, μ and σ. Dominance of larger mean volume diameter (D_m) values was observed during the second event.

The $N_T - R$ relationship has been modelled separately for all the phases of the events (figure 22a–b). It is evident that the empirical

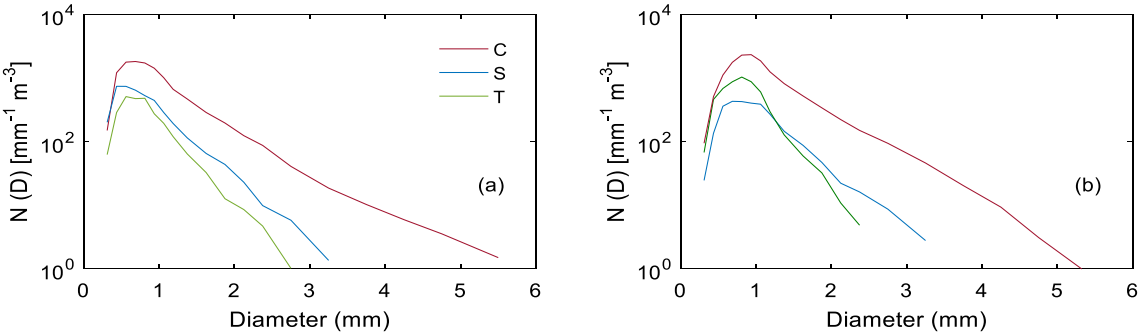

Figure 20. Number concentration of raindrop during squall event on (**a**) April 1, 2018 and (**b**) April 7, 2018.

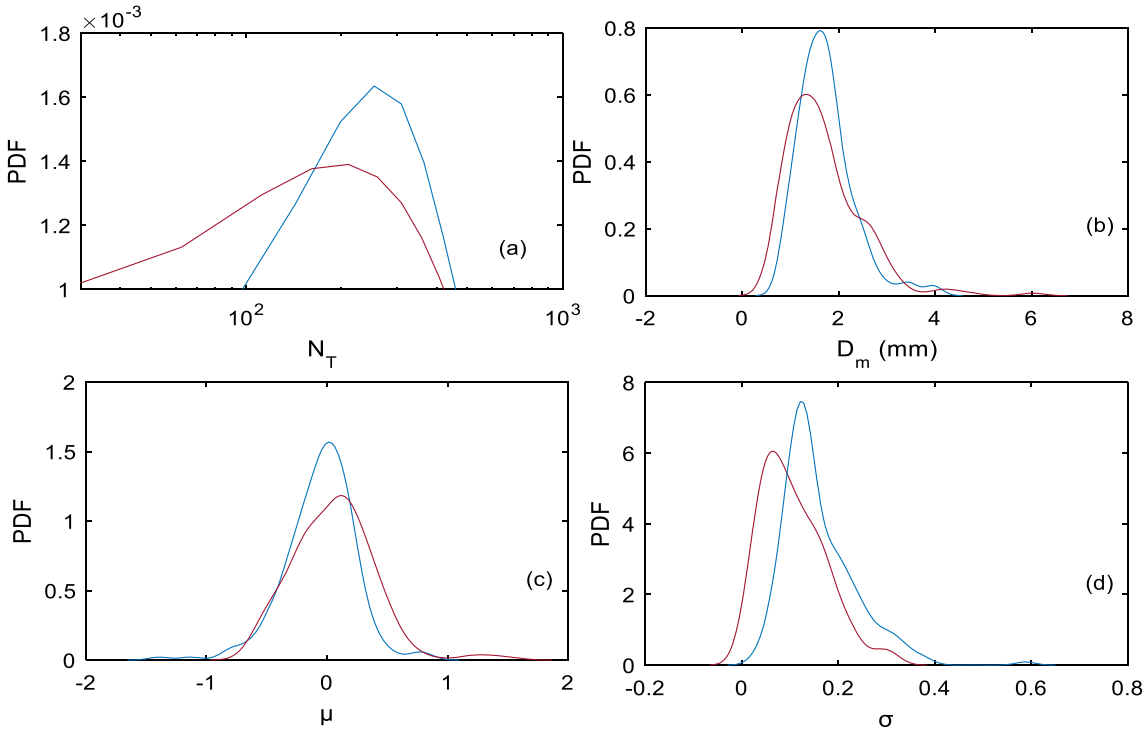

Figure 21. Distribution of (**a**) N_{T}, (**b**) D_{m}, (**c**) μ, and (**d**) σ during the two squall events.

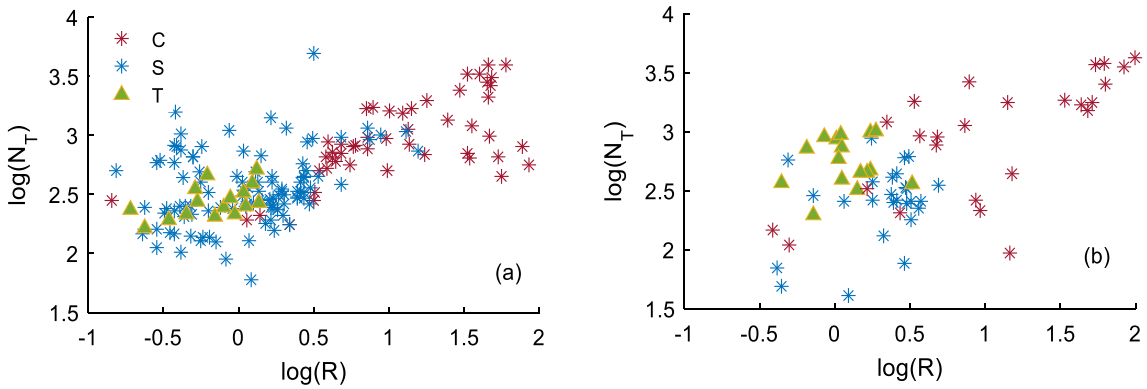

Figure 22. N_{T}–R relation for the rain during the squall events on (**a**) April 1, 2018 and (**b**) April 7, 2018.

relation is notably different for the three said spells for both the events. However, the separation is a little better for the second event.

The connection between radar reflectivity and rain intensity happens to be extremely crucial in the performance of radar-based QPE (quantitative precipitation estimation). The Z–R relationships for the two events were studied next to visualise their impact on the said relationship. The empirical coefficients a were found to be exceptionally high for both the events, which indicates high degree of convection in the events (figure 23). Ochou *et al.* (2011) also reported such large value of coefficient a in strong thunderstorms. The a values were even larger in the second event (1995) than in the first one (1584), which finds good agreement with the abundance of large drops reported in the second event.

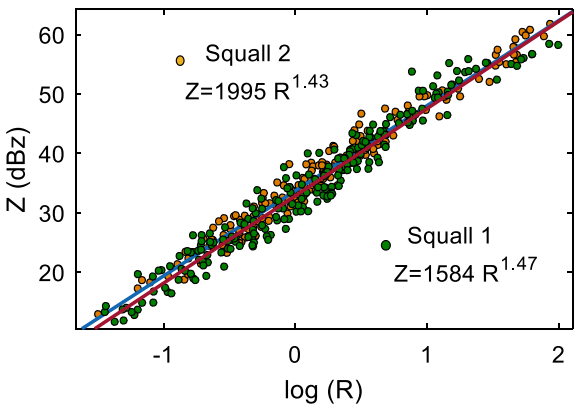

Figure 23. Empirical relationship between Z and R during the two squall events.

The use of higher frequencies has facilitated detailed understanding of different atmospheric processes, e.g., GPM satellite provides global rain monitoring at a Ka and Ku band frequency. However, frequencies above 10 GHz are attenuated largely due to rain. Here, the path attenuation caused by the two squall events has been modelled using the DSD. The path attenuation seemed to be larger during the first squall event for both the frequencies used by GPM satellite (13.6 and 35.5 GHz). Figure 24(a–b) shows the empirical relationships between path attenuation and rain intensity. The coefficients k and $\acute{\alpha}$ were found to be 0.08 and 1.14 for the first event, whereas the values for the second one were 0.03 and 1.26 at 13.6 GHz. The coefficients at the higher frequency band used by GPM (35.5 GHz) were found to be 0.53 and 0.89 for the first squall, while the values were 0.31 and 0.92 in case of the second unconventional squall.

4. Conclusion

The current work has presented a thorough study of two squall events with nearly similar severity but different organisational modes. The first event showed a leading convective spell, whereas the second one had a leading stratiform phase followed by a convective line, unlike usual squall systems. Both the events showed large variations in synoptic weather conditions, e.g., in atmospheric temperature drop and wind speed increase during the squall passages. The lightning activities were slightly more intense during the latter. Even though the wind gusts were comparable, the gust was experienced by

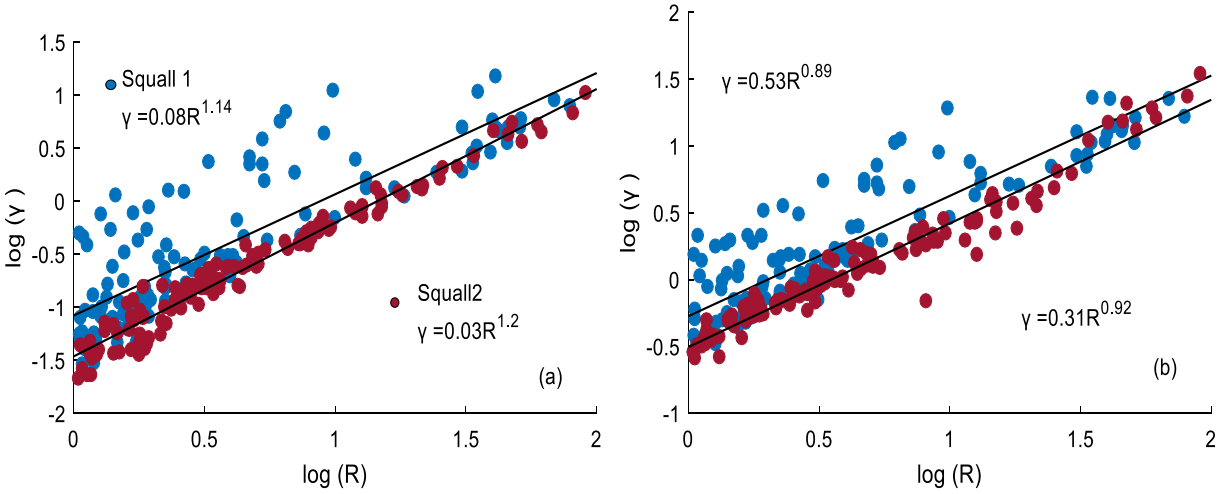

Figure 24. Relation between specific path attenuation (dB/km) and rain intensity for the two squall events at (**a**) 13.6 GHz and (**b**) 35.5 GHz.

a larger area during the second storm. The increase in CAPE and OLR drops was significant during both the events. The first one was found to have a breakage of storm front, which probably contributed to higher CAPE surrounding the study location, even though the localised value was slightly higher during the second event. The short-lived second squall having an unconventional organisational mode, presented weaker vertical wind shear in spite of having dense lightning activities. Both the events had significantly dense cloud mask and large cloud optical thickness over the city, with the second event showing slightly higher values. Dominance of smaller cloud ice particles and low-pressure cloud tops have been witnessed in the second day's precipitation system. DSD parameters in convective, stratiform and 'T' phases of the events were clearly distinguishable in both the events. The 'T' region showed lesser number of drops than the strartiform phase for the first case, whereas the reverse scenario was observed in the latter. Exceptionally high a values in empirical relation between Z and R were noticed in both the cases. The study reports higher path attenuation during the first event. This study has manifested the presentation of an unconventional squall event and its distinction from a traditional tropical squall. Besides, all the synoptic and microphysical properties have been analysed in detail. The work indicated that even though the predictability of mesoscale systems using different atmospheric features can be highly beneficial for the prediction of mesoscale systems, the efficiency of such predictability can have complex variations, especially during unconventional convective development. This can be useful in a better understanding of the rare mesoscale events over tropics. However, it is not possible to comment on the generalised distinctions between the two different organisational modes discussed here in the current study. The study of a statistically robust dataset with different organisational modes of squalls comes under the future aim of this work.

Acknowledgements

The authors wish to thank the World Wide Lightning Location Network (http://wwlln.net), a collaboration among over 50 universities and institutions, for providing the lightning data used in this paper. The authors also thankfully acknowledge the official website of ISRO and ECMWF for providing access to the datasets used.

Author statement

Both authors contributed to the study and have read and approved the final manuscript.

References

Altaratz O, Koren I, Yair Y and Price C 2010 Lightning response to smoke from Amazonian fires; *Geophys. Res. Lett.* **37(7)**.

Betts A K 1976 The thermodynamic transformation of tropical sub-cloud layer by precipitation and downdrafts; *J. Atmos. Sci.* **30** 1008–1020.

Betz H, Price C and Di Paola F 2013 Using a cloud electrification model to study relationships between Atmospheric lightning activity and cloud microphysical structure; *Nat. Hazards Earth Syst. Sci.* **13** 1085–1104.

Buiat M, Porcu F and Dietrich S 2017 Observing relationships between lightning and cloud profiles by means of a satellite-borne cloud radar; *Atmos. Meas. Tech.* **10** 221–230.

Carvalho K S and Wang S 2019 Characterising the Indian Ocean sea level changes and potential coastal flooding impacts under global warming; *J. Hydrol.* **569** 373–386.

Chatterjee C and Das S 2020 On the association between lightning and precipitation microphysics; *J. Atmos. Sol.-Terr. Phys.* **207(105350)**, https://doi.org/10.1016/j.jastp.2020.105350.

Chaudhari H S, Sawaisarje G K and Ranalkar M R 2010 Thunderstorms over a tropical Indian station, Minicoy: Role of vertical wind shear; *J. Earth Syst. Sci.* **119** 603–615.

Dalal S, Lohar D, Sarkar S, Sadhukhan I and Debnath G 2012 Organisational modes of squall-type mesoscale convective systems during pre-monsoon season over eastern India; *Atmos. Res.* **106** 120–138.

Das S, Maitra A and Shukla A 2010 Rain attenuation modeling in the 10–100 GHz frequency using drop size distributions for different climatic zones in tropical India; *Progr. Electromag. Res.* **25** 211–224.

De U, Dube R and Prakasa G 2005 Extreme weather events over India in the last 100 years; *J. Ind. Geophys. Union* **9** 173–187.

Hamilton R A and Arch-bold J W 1945 Meteorology of Nigeria and adjacent territory; *Quart. J. Roy. Meteorol. Soc.* **71** 231–264.

Huschke R E 1959 *Glossary of meteorology*; Boston American Meteorological Society.

Ippolito L J 1986 *Radio wave propagation in satellite communication*; Van Nostrand Reinhold Company, New York.

Johns R H and Doswell C A 1992 Severe local storms forecasting; *Wea. Forecast* **7** 588–612.

Kozu T and Nakamura K 1991 Rainfall parameter estimation from dual-radar measurements combining reflectivity profile and path-integrated attenuation; *J. Atmos. Ocean. Technol.* **8(2)** 259–270.

Lay E, Holzworth R, Rodger C, Thomas J, Pinto J and Dowden R 2004 WWLL global lightning detection system: Regional validation study in Brazil; *Geophys. Res. Lett.* **31**.

Liebmann B and Smith C A 1996 Description of a complete (interpolated) outgoing longwave radiation dataset; *Bull. Am. Meteorol. Soc.* **77** 1275–1277.

Makela A 2004 Comparison between lightning data and cloud top temperatures in Finland; EUMETSAT Conference Proceeding.

Marwitz J D 1972 The structure and motion of severe hailstorms. Part III: Severely sheared storms; *J. Appl. Meteorol. Climatol.* **11(1)** 189–201.

Midyas S, Pal S, Dutta R, Gole P, Chattopadhyay G, Karmakar S, Saha U and Hazra S 2021 A preliminary study on pre-monsoon summer thunderstorms using ground-based total lightning data over Gangetic West Bengal; *Ind. J. Phys.* **95(1)**, https://doi.org/10.1007/s12648-020-01681-y.

Mishra A K, Nagaraju V, Rafiq M and Chandra S 2018 Evidence of links between regional climate change and precipitation extremes over India; *Weather* **99**.

Molinie G and Jacobson A R 2004 Cloud-to-ground lightning and cloud top brightness temperature over the contiguous United States; *J. Geophys. Res.* **109(D13106)** 1–16.

Moussa A, Diop B, Wade M, Abdoulaye S, Abdoulaye D, Aichetou D, Sarr D and Abdou F 2019 Case study of squall lines passing over Dakar using NOAA sounders; *Int. J. Sci. Res.* **8** 272–276.

Mukhopadhyay P, Mahakur M and Singh H A K 2009 The interaction of large scale and mesoscale environment leading to formation of intense thunderstorms over Kolkata. Part I: Doppler radar and satellite observations; *J. Earth Syst. Sci.* **118** 441, https://doi.org/10.1007/s12040-009-0046-1.

Nakazawa T 2006 Madden–Julian oscillation activity and typhoon landfall on Japan in 2004; *SOLA* **2** 136–139.

Nayak H P and Mandal M 2014 Analysis of stability parameters in relation to precipitation associated with pre-monsoon thunderstorms over Kolkata, India; *J. Earth Syst. Sci.* **123** 689–703.

Ochou A, Zahiri E, Bamba B and Koffi M 2011 Understanding the variability of Z–R relationships caused by natural variations in raindrop size distributions (DSD): Implication of drop size and number; *Atmos. Clim. Sci.* **1(3)** 147–164.

Özdemir E, Yavuz V, Deniz A, Karan H, Kartal M, Kent S 2019 Squall line over Antalya: A case study of the events of 25 October 2014; *Weather* **74.**

Parker M and Johnson R H 2000 Organizational modes of midlatitude mesoscale convective systems; *Month. Wea. Rev.* **128(10)** 3413–3436.

Platnick S, P Hubanks, K Meyer and King M D 2015 MODIS Atmosphere L3 Monthly Product (08_L3) NASA MODIS; Adaptive Processing System, Goddard Space Flight Center.

Pucik T, Groenemeijer P and Tsonevsky I 2021 Vertical wind shear and convective storms; *ECMWF*, https://doi.org/10.21957/z0b3t5mrv.

Rotunno R, Klemp J B and Weisman M L 1988 A theory for strong, long-lived squall lines; *J. Atmos. Sci.* **45(3)** 463–485.

Saylor J R, Ulbrich C W, Ballentine J W and Lapp J L 2005 The correlation between lightning and DSD parameters; *IEEE Trans. Geosci. Remote Sens.* **43(8)** 1806–1815.

Schiro K, Neelin J, Adams D and Lintner B 2016 Deep convection and column water vapor over tropical land *vs.* Tropical Ocean: A comparison between the Amazon and the Tropical Western Pacific; *J. Atmos. Sci.* **73**.

Singleton A and Toumi R 2013 Super-Clausius–Clapeyron scaling of rainfall in a model squall line; *Quart. J. Roy. Meteorol. Soc.* **139** 334–339.

Solomon R, Medaglia C, Adamo C, Dietrich S and Mugnai A 2003 Relating cloud microphysical properties and lightning: Model analysis of an extreme hailstorm; *Proc. 5th EGS Plinius Conference*, France.

Timothy K, Ong J and Choo E 2002 Raindrop Size Distribution Using Method of Moments for Terrestrial and Satellite Communication Applications in Singapore; *IEEE Trans. Ant. Propagation* **50(10)**.

Tokay A and Short D A 1996 Evidence from tropical raindrop spectra of the origin of rain from stratiform versus convective clouds; *J. Appl. Meteor.* **35** 355–371.

Vidyarthi A, Jassal B S, Ieee R G M and Shukla A 2011 Comparison between empirical lognormal and gamma rain drop-size distribution models for Indian Region; *Proc. Asia-Pacific Microwave Conference*, pp. 1686–1689.

Wang Z, Lin L and Zhang X *et al.* 2017 Scenario dependence of future changes in climate extremes under 1.5°C and 2°C global warming; *Sci. Rep.* **7**, https://doi.org/10.1038/srep46432.

Zhao B, Jiang J H, Gu Y, Diner D, Worden J, Liou K N, Su H, Xing J, Garay M and Huang L 2017 Decadal-scale trends in regional aerosol particle properties and their linkage to emission changes; *Environ. Res. Lett.* **12**, https://doi.org/10.1088/1748-9326/aa6cb2.

Zipser E J 1969 The role of organised unsaturated convective downdrafts in the structure and rapid decay of an equatorial disturbance; *J. Appl. Meteorol.* **8(5)** 799–814.

Zipser E J 1977 Mesoscale and convective-scale downdrafts as distinct components of squall-line structure; *Mon. Wea. Rev.* **105(12)** 1568–1589.

Corresponding editor: Parthasarathi Mukhopadhyay